International Journal of Pharmaceutics

Volume 530, Issues 1–2, 15 September 2017, Pages 139-144

https://doi.org/10.1016/j.ijpharm.2017.07.053

Variable-focus microscopy and UV surface dissolution imaging as complementary techniques in intrinsic dissolution rate determination

Adam Ward[a], Karl Walton[b], Karl Box[c], Jesper Østergaard[d], Lisa J. Gillie[e], Barbara R. Conway[a], Kofi Asare-Addo[a]*,

[a]Department of Pharmacy, University of Huddersfield, Huddersfield, HD1 3DH, UK

[b]EPSRC Centre for Innovative Manufacturing in Advanced Metrology, University of Huddersfield, Huddersfield, HD1 3DH, UK

[c]Sirus Analytical, Riverside, Forest Row Business Park, Station Road, Forest Row, RH18 5DW

[d]Department of Pharmacy, University of Copenhagen, Universitetsparken 2, DK-2100 Copenhagen

[e]Department of Chemical Sciences, University of Huddersfield, Huddersfield, HD1 3DH, UK

*Corresponding author (Kofi Asare-Addo)

e-mail: k.asare-addo@hud.ac.uk

Tel: +44 1484 472360

Graphical Abstract

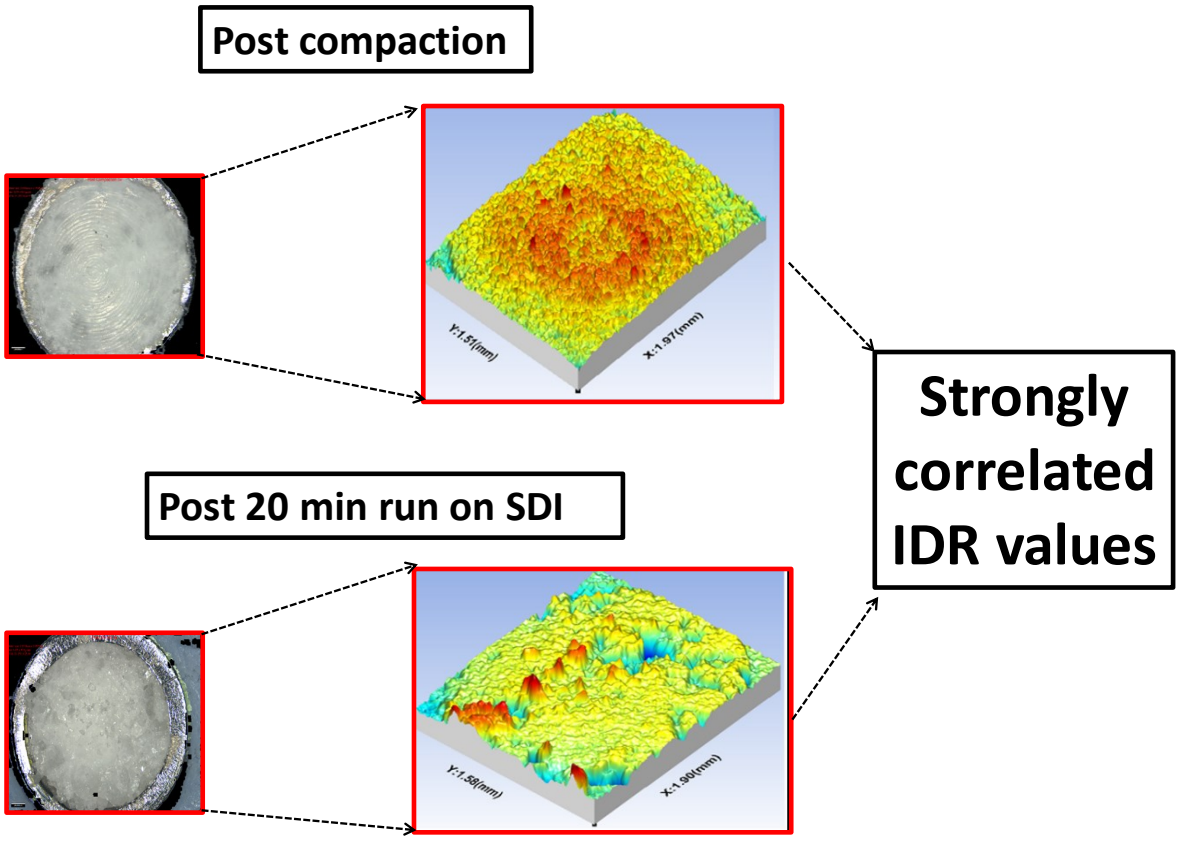

Highlights

- **No form changes in ibuprofen after SDI run**
- **Decrease in intrinsic dissolution rate of ibuprofen from 10 min to 20 min**
- **Post-flush effective in removing trapped air bubbles**
- **Surface parameters generated by variable-focus microscope showed key trend with intrinsic dissolution values seen from UV-imaging**

Abstract

This work reports a novel approach to the assessment of the surface properties of compacts used in Surface Dissolution Imaging (SDI). SDI is useful for determining intrinsic dissolution rate (IDR), an important parameter in early stage drug development. Surface topography, post-compaction and post-SDI run, have been measured using a non-contact, optical, three-dimensional microscope based on focus variation, the Alicona Infinite Focus Microscope, with the aim of correlating the IDRs to the surface properties. Ibuprofen (IBU) was used as a model poorly-soluble drug. DSC and XRD were used to monitor possible polymorphic changes that may have occurred post-compaction and post-SDI run. IBUs IDR decreased from 0.033 mg/min/cm^2 to 0.022 mg/min/cm^2 from 10 to 20 min, respectively, during the experiment. XRD and DSC showed no form changes during the SDI run. The surface topography images showed that a distinct imprint was embossed on the surfaces of some compacts which could affect IDRs. Surface parameter values were associated with the SDI experiments which showed strong correlations with the IDR values. The variable-focus microscope can be used as a complimentary tool in the determination of IDR values from the SDI.

Keywords: Ibuprofen; Intrinsic dissolution rate; Surface dissolution imaging; Alicona infinite microscope; Surface roughness; Polymorphism.

Abbreviations: IBU, Ibuprofen; USP, United Sates Pharmacopeia; SDS, Sodium dodecyl sulphate; DSC, differential scanning calorimetry; XRPD, x-ray powder diffraction; IDR, Intrinsic dissolution rate; SDI, Surface dissolution imaging; API, Active pharmaceutical ingredient.

1. Introduction

Intrinsic dissolution rate (IDR) is an important parameter determined in early stage drug development that helps to predict API in vivo behaviour. The crystallites of the compounds orientate less randomly during their compression and although it is suggested that the preferred orientation of crystallites has a weak correlation with its IDR, it is something that must be considered during accurate dissolution studies (Löbmann et al., 2014; Techno et al., 2007). Cornell et al. 1974 showed that the different faces of crystals depending on their sizes have different contributions to the total surface area and hence their dissolution which means some faces dissolving more quickly than others. Macpherson et al. (1996) also determined the kinetics and mechanism controlling dissolution from the (100) cleavage face of potassium bromide single crystals in acetonitrile using a novel integrated electrochemical/AFM probe and a scanning electrochemical microscope. Other authors have looked at milling, anisotropic surface energetics and wettability of paracetamol crystals (Heng et al., 2006; Heng at al., 2006a). The Surface Dissolution Imaging (SDI) instrument with Actipix™ Technology (Sirius Analytical, Forest Row, UK) offers a compound sparing approach requiring typically 5 - 10 mg of API and an experimental run time of 20-30 min in determining the IDR of an API. Several authors have used the SDI in monitoring IDRs of APIs (Niederquell and Kuentz, 2014; Boetker et al., 2013; Gordon et al., 2013; Hulse et al., 2012; Qiao et al., 2013) as well as in other applications (Ostergaard, et al., 2014, 2010; Ye & Yaghmur, 2011) but to date there has been no work looking at how the surface properties of materials can impact the IDR values obtained. The Alicona™ microscope (Alicona Imaging GmbH, Graz, Austria) is a non-contact optical 3D micro-coordinate measurement and surface texture assessment instrument which operates on the focus variation principle. The technology is typically used for quality assurance in micro-precision manufacturing (Walton et al., 2016; 2015; 2014) and is capable of acquiring topographic surface height data in profile (2D) and areal (3D) formats along with true colour surface images. This work reports on the novel use of the Alicona™ instrument to

assess the topography of compact surfaces post-compaction and post-SDI run with the objective of standardising SDI procedures and thus providing consistency in IDR determination.

2. Materials and Methods

Ibuprofen (commercial IBU or bulk powder) and sodium dodecyl sulphate (SDS) were purchased from Sigma (UK).

The SDI with with Actipix™ Technology (Sirius Analytical, Forest Row, UK) was used in the determination of IDR. The IDR values are calculated using the software which takes the nominal area of the disk used into consideration. A consistent mass of API (5 mg) was used for each compact (compact holder inner diameter is 2 mm and height 2.4 mm) and the torque was applied using a set number of turns of the Allen key.

A 1% w/v SDS solution was used as dissolution medium at a flow rate of 0.2 mL/min at 37 °C applying a wavelength of 214 nm. The molar extinction coefficient of IBU was experimentally determined to be 7596.5 $M^{-1}cm^{-1}$ with an r^2 value of 0.9925 using a concentration range of 0.000005 - 0.001 M. Samples were run for 10 or 20 min. Experiment were conducted in triplicates.

Prior to surface assessment with a x5 objective lens on the focus variation microscope (Alicona™ microscope (Alicona Imaging GmbH, Graz, Austria), the SDI compacts were dried in an oven at a constant temperature of 40 °C for 20 min to offset any adverse optical effects from liquid films. This procedure was conducted for all compacts post-compaction, post-flush on SDI, post-10 min run and post-20 min run. The obtained images were analysed using the Surfstand™ software (Taylor Hobson,UK, and University of Huddersfield, UK). A schematic representation of the zoom analysis of the compact surface and a software view are shown in Figure 1. The significant parameters used in describing compact surfaces were; highest peak (S_p), lowest valley (S_v), distance between the highest and lowest points (S_z) (Figure 1c shows S_z determination) and the developed interfacial (surface) area ratio (S_{dr}). The developed interfacial area ratio is a measure of the true

surface area of the textured sample compared to that of a uniform flat surface. It is expressed as a percentage by which the true measured surface area exceeds that of the nominal uniform measurement area. S_{dr} was calculated from equation 1.

$$Sdr = \frac{(Texture\ Surface\ Area) - (Cross\ Sectional\ Area)}{Cross\ Sectional\ Area} \quad \text{Equation 1}$$

SDI compacts after variable focus microscopy, were scanned from 5° to 100° 2theta at a rate of 1.5° min^{-1} using a Bruker D2 Phaser benchtop x-ray powder diffractometer. The bulk powder was analysed using a plastic well plate. For analysis of the compacts, the powder held in the stainless steel cup was directly placed on a silica wafer, spread out using a spatula and directly analysed. This technique was implemented due to the small amount of powder contained in the stainless steel cup. All samples were analysed by differential scanning calorimetry (DSC822E, Mettler-Toledo, Switzerland) after XRPD analysis using standard aluminium pans (40 µL) with a vented lid. The pans were heated from 25 to 220 ˚C at a rate of 10 °C/min while purging using nitrogen gas. The enthalpy, onset temperatures and melting points of the samples were obtained (a detailed account of the material and method section can be found in the supplementary section).

3. RESULTS AND DISCUSSION

The post-flush images highlight how effective the system is at removing trapped air bubbles (indicated by black arrows) shown in Figure 2a. The post-flush images also indicate that dissolution is occurring to some extent before the experiment is recorded. During the 10 min run (Figure 2b), a significant 'wave' was seen above the usual jet stream (indicated by red arrow). Wave development may be a consequence of several processes such as removal of surface particles, erosion of layers of the compact caused by lamination and the surface of the compact itself causing disturbance in the laminar flow of the system. The sample run at the 20 min time period (Figure 2c) also resulted in wave generations (indicated by orange arrow) in the jet stream, similar to the 10 min. Figure 2d

130 shows a representative IDR v time graph for a 10 min SDI run. The significant wave resulted in
131 relatively bigger error margins in the 2-4 min region thus highlighting the objective of standardising
132 SDI procedures to provide consistency in IDR determination. As indicated in figure 2 and table 1,
133 IDR decreased over time. The IDRs given in table 1 were calculated using the nominal area of the
134 flat disk (A = 3.14 mm^2). Also, as discussed below, the errors due to surface roughness and area
135 changes during dissolution are inherently associated with these values. The focus of this current
136 work was the investigation of the relationship between the relative changes in surface
137 area/roughness and IDR. As such, the authors did not investigate and compare IDR values extracted
138 from the images and from effluent data. This subject remains underexplored presumably because
139 the main interest, at least in an industrial setting, is rank ordering of compounds with respect to
140 dissolution performance and to a lesser extent the absolute IDRs. A few studies however, have
141 addressed the quantitative performance of the SDI system in terms of IDR determination. The level
142 of agreement however has been variable depending drug compound in question (Madelung et al.,
143 2017; Ostergaard et al., 2014; Boetker at al., 2013).

144 XRPD (Figure 3a) and DSC (not included) confirmed no changes had occurred to the IBU during
145 the compaction and SDI run processes. The compaction process however, increased the crystallinity
146 of the bulk IBU powder. Figure 3b also shows the scanning electron microscopy (SEM) image of
147 depicting the crystal habit of the ibuprofen crystal. The post-compaction images (Figure 4a) from
148 the focus variation microscope highlight two key observations. The first was that some amount of
149 the IBU powder had been compacted on to the steel rim (Figure 4a, highlighted by the red arrow)
150 with the second being that a distinct imprint of the die remained on the compacts surface (indicated
151 by blue arrow). The consequences could be increased disruption of flow within the SDI and the
152 dissolution of the API from the rim first rather than the surface of the compact. In the post-flush
153 images (Figure 4b), it can be seen that excess API has been removed from the steel rim surrounding

154 the compact and that dissolution had occurred to some extent, increasing the valley depth on the
155 surface.

156 The S_{dr} value of 0.03 for the post compaction compact indicates a closer similarity to the true plane
157 of the surface area that should be produced by the uniform flat surface. The post flush process
158 increases the S_{dr} value to 0.50 and this can be reflected in the increase of the highest peak (Sp) and
159 lowest valley (Sv) (Table 1) causing a significant increase in the distance between the highest peaks
160 and lowest valley (68 to 423 μm). This key trend was evident for the 10 and 20 min sample also.
161 There is a gradual decrease in area from the post flush samples up to the 20 min sample for all the
162 surface parameters measured. The calculated surface properties again at the 10 min and 20 min SDI
163 runs shows a key trend with the IDR values. The Surfstand^{TM} images of representative compacts of
164 IBU in figure 5 relate to Table 1 and confirm the changes in the surface parameters. Figure 5a
165 shows the relatively smoother surface post compaction with figure 5b showing the relatively
166 rougher surfaces and increased surface area as a result of the post-flush. The darker blue valleys in
167 figure 5b and c could account for the significant wave seen in the jet stream in Figure 2. Figure 5d
168 shows the surfaces becoming smoother post the 20 min run. The ability to determine these
169 parameters therefore offers an insight into how surface changes of the compact relate to IDR
170 measurements in trying to get consistent values.

171

172 **4. CONCLUSIONS**

173 XRD and DSC showed no changes to occur in the IBU compacts post SDI runs. IDR values
174 decreased for IBU as the length of the run was increased from 10 min to 20 min. The focus
175 variation microscopy revealed that changes occurring on the compact surfaces paralleled changes in
176 IDR values. It showed a decrease in surface area of the compacts from post-flush to the 20 min run
177 related to a decrease in the IDR values. The ability to determine these parameters therefore offers an

178 insight into how surface changes of the compact relate to IDR measurements and could further
179 impact decisions made in the preformulation stage of drug discovery.

180

181 **5. ACKNOWLEDGEMENTS**

182 The authors would like to acknowledge the University of Huddersfield for financial support and
183 Paul Whittles of Sirius Analytical for the kind use of the SDI instrument.

184

185 **6. REFERENCES**

186 Boetker, J. P., Rantanen, J., Rades, T., Müllertz, A., Østergaard, J., Jensen, H. 2013. A new
187 approach to dissolution testing by UV imaging and finite element simulation. Pharm Res 30:1328–
188 1337.

189 Cornell, R. M., Posner, A. M., & Quirk, J. P. 1974. Crystal morphology and the dissolution of
190 goethite. J. Inorg. Nucl. Chem 36(9), 1937-1946.

191 Gordon, S., Naelapää, K., Rantanen, J., Selen, A., Müllertz, A., Østergaard, J. 2013. Real-time
192 dissolution behavior of furosemide in biorelevant media as determined by UV imaging. Pharm Dev
193 Technol 18:1407–1416.

194 Heng, J. Y. Y., Bismarck, A., Lee, A. F., Wilson, K., Williams, D. R. 2006. Anisotropic surface
195 energetics and wettability of macroscopic form I paracetamol crystals. *Langmuir*, *22*(6), 2760-2769.

196 Heng, J. Y. Y., Thielmann, F., Williams, D. R. 2006a. The effects of milling on the surface
197 properties of form I paracetamol crystals. Pharm Res, 23(8), 1918-1927.

198 Hulse, W. L, Gray, J., Forbes, R. T. 2012. A discriminatory intrinsic dissolution study using UV
199 area imaging analysis to gain additional insights into the dissolution behaviour of active
200 pharmaceutical ingredients. Int J Pharm 434:133–139.

201 Löbmann, K., Flouda, K., Qiu, D., Tsolakou, T., Wang, W., Rades, T. 2014. The influence of
202 pressure on the intrinsic dissolution rate of amorphous indomethacin. *Pharmaceutics*, *6*(3), 481-
203 493.

204 Macpherson, J. V., Unwin, P. R., Hillier, A. C., Bard, A. J. 1996. In-situ imaging of ionic crystal
205 dissolution using an integrated electrochemical/AFM probe. J. Am. Chem. Soc., 1996, 118 (27),
206 6445-6452

207 Niederquell, A., & Kuentz, M. 2014. Biorelevant dissolution of poorly soluble weak acids studied
208 by UV imaging reveals ranges of fractal-like kinetics. Int J Pharm (1), 38-49.

209 Ostergaard, J., Wu, J. X., Naelapaa, K., Boetker, J. P., Jensen, H., & Rantanen, J. 2014.
210 Simultaneous UV imaging and Raman spectroscopy for the measurement of solvent-mediated phase
211 transformations during dissolution testing. J Pharm Sci (103), 1149-1156.

212 Ostergaard, J., Meng-Lund, E., Larsen, S. W., Larsen, C., Karsten, P., Lenke, J., & Jensen, H. 2010.
213 Real time UV imaging of nicotine release from transdermal patches. Pharm Res, 2614-2623.

214 Qiao, N., Wang, K., Schlindwein W., Davies, A., Li, M. 2013. In situ monitoring of carbamazepine-
215 nicotinamide cocrystal intrinsic dissolution behaviour. Eur J Pharm Biopharm 83:415–426.

216 Tenho, M.; Heinänen, P.; Tanninen, V.P.; Lehto, V.-P. 2007. Does the preferred orientation of
217 crystallites in tablets affect the intrinsic dissolution? J. Pharm. Biomed. Anal. 43, 1315–1323.

218 Walton, K., Fleming, L., Goodhand, M., Racasan, R., & Zeng, W. 2016. High fidelity replication of
219 surface texture and geometric form of a high aspect ratio aerodynamic test component. Surface
220 Topography: Metrology and Properties, 4(2), 025003.

Walton, K., Blunt, L., & Fleming, L. 2015. The topographic development and areal parametric characterization of a stratified surface polished by mass finishing. Surface Topography: Metrology and Properties, 3(3), 035003.

Walton, K., Blunt, L., Fleming, L., Goodhand, M., & Lung, H. 2014. Areal parametric characterisation of ex-service compressor blade leading edges. Wear, 321, 79-86.

Ye, F., & Yaghmur, A. 2011. Real-time UV imaging of drug diffusion and release from Pluronic F127 hydrogels. Eur J Pharm Sci, 236-243.

241 Table 1. Calculated intrinsic dissolution rate (IDR) and surface properties from Surfstand™ for

242 Ibuprofen (n = 3)

Compact	Intrinsic dissolution rate (IDR) (mg/min/cm^2)	Parameter			
		Developed Interfacial (Surface) Area Ratio (S_{dr})	Highest Peak Sp (µm)	Lowest Valley Sv (µm)	Distance between Sz (µm)
Post compaction	-	1.03± 0.8	23 ± 5	42 ± 16	80 ± 24
Post flush	-	1.50 ± 1.2	298 ± 28	232 ± 48	495 ± 48
Post 10 min run	0.033 ± 0.004	1.41 ± 0.9	212 ± 36	212 ± 17	409 ± 12
Post 20 min run	0.022 ± 0.001	1.22 ± 5.3	99 ± 10	91 ± 11	218 ± 28

243

244

245

246

247

248

249

250

251

252

253

254

255 **Figure captions**

256 **Figure 1**. (a) Schematic representation of the zoom analysis of the compact surface in variable-
257 focus microscopy, (b) software view using Surfstand^{TM} when zooming in on the **same** surface of a
258 carbamazepine sample, (c) schematic of Surfstand^{TM} parameters as used in Table 1.

259 **Figure 2**. Surface Dissolution Imaging of IBU (a) post flush (start point was at 1 s, mid-point at 5 s
260 and end-point at 10 s), (b) after 10 min (start point was at 1 min, mid-point at 5 min and end-point
261 at 10 min), (c) after 20 min (start point was at 1 min, mid-point at 10 min and end-point at 20 min),
262 (d) intrinsic dissolution rate as a function of time for the 10 min SDI run (Image inserts show area
263 of significant wave development causing big errors from 2-4 min). Error bars indicate high
264 variability that can occur at the different time points in IDR determinations due to the variability on
265 the surface of compacts.

266 **Figure 3**. (a) XRPD of IBU samples of the commercial ibuprofen (bulk powder), post compaction,
267 post flush on the SDI and after 10 and 20 min run on the SDI, (b) SEM image depicting the crystal
268 habit of ibuprofen

269 **Figure 4**. Focus variation (Alicona^{TM}) 3D data set images of representative compacts of IBU (a)
270 post compaction, (b) post flush, (c) after 10 min run on SDI, (d) after 20 min run on SDI. Note:
271 diameter of sample holder in image is 2.5 mm (measured using a 150 mm digital calliper gauge
272 from Draper Tools Ltd, UK).

273 **Figure 5**. Surfstand^{TM} images of representative compacts of IBU (a) post compaction, (b) post
274 flush, (c) after 10 min run on SDI, (d) after 20 min run on SDI. Note: highest peaks and lowest
275 valleys values on these images are tabulated in Table 1.

276

277

Figures

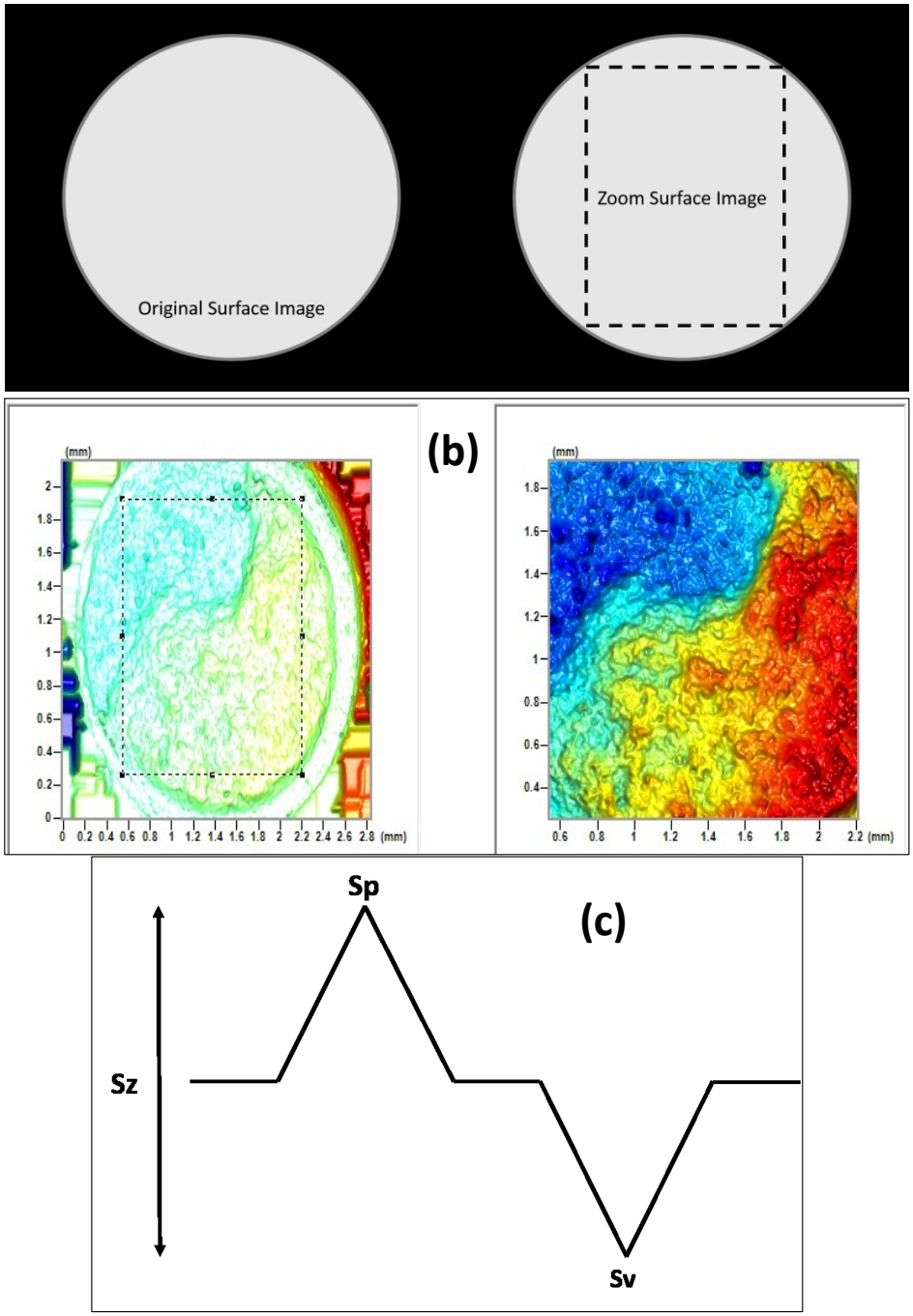

Figure 1.

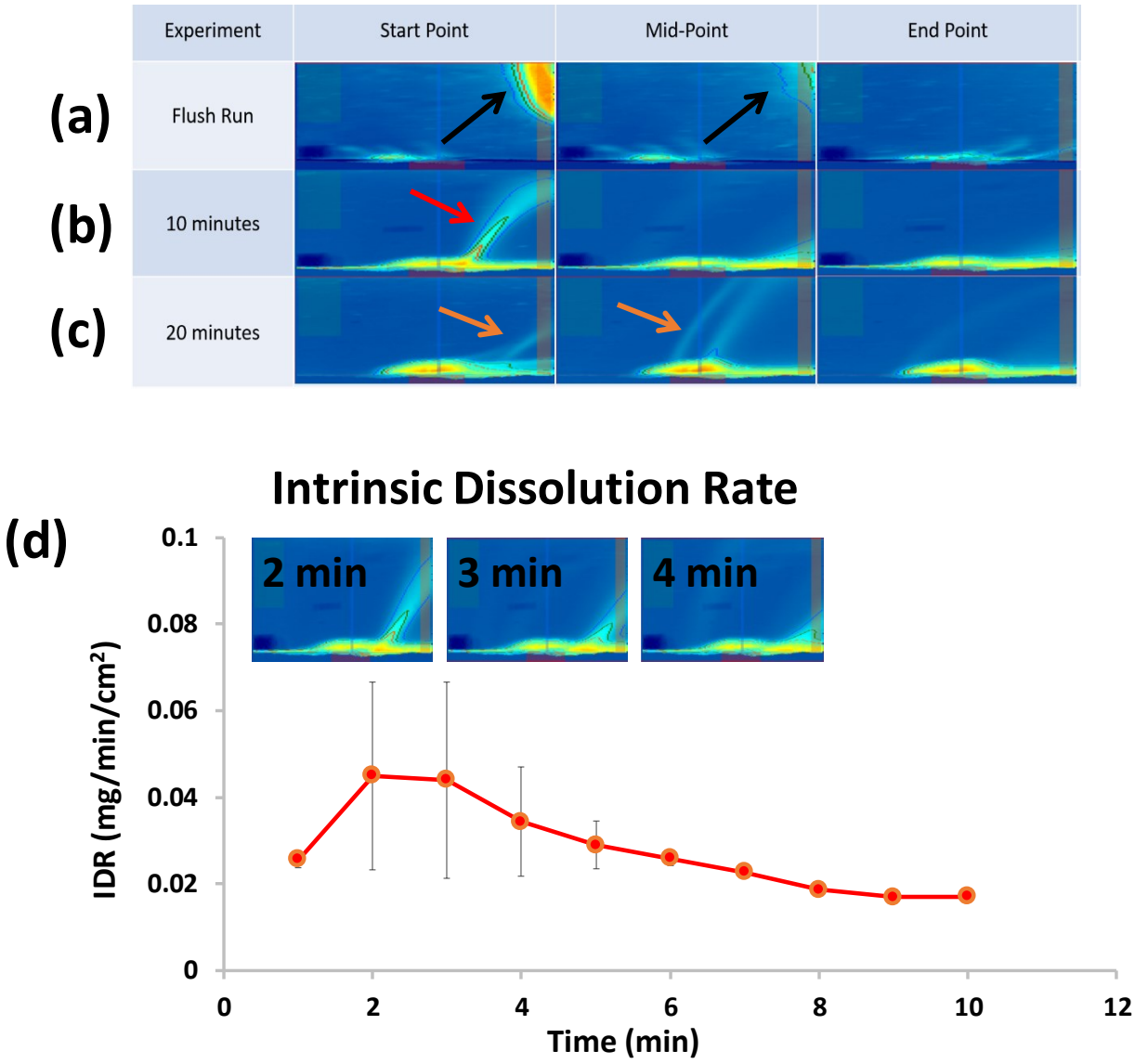
Experiment
Start Point
Mid-Point
End Point
(a)
Flush Run
(b)
10 minutes
(c)
20 minutes
(d)
Intrinsic Dissolution Rate
2 min
3 min
4 min
IDR (mg/min/cm²)
0.1
0.08
0.06
0.04
0.02
0
0
2
4
6
8
10
12
Time (min)

Figure 2.

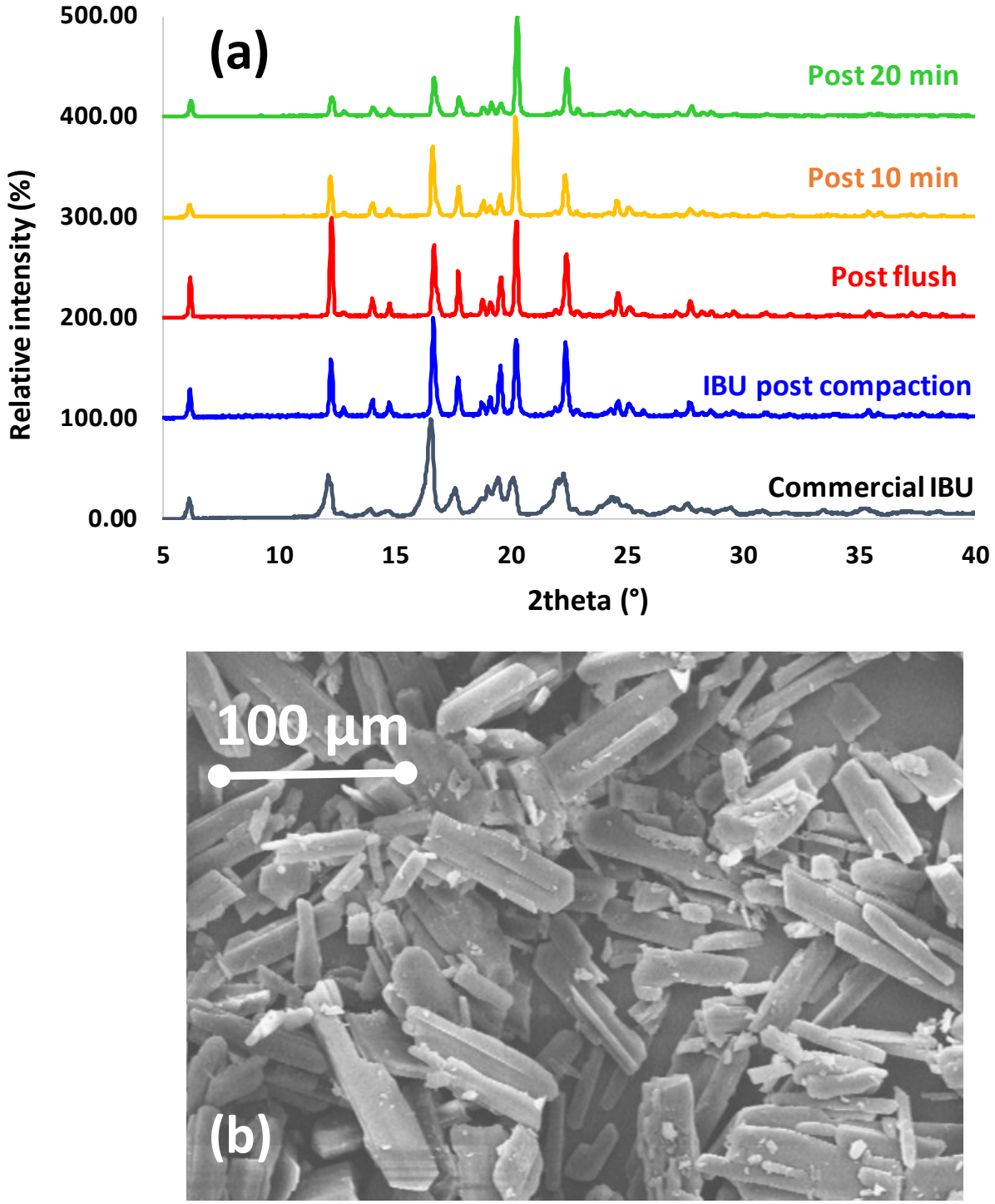
(a)
Post 20 min
Post 10 min
Post flush
IBU post compaction
Commercial IBU
Relative intensity (%)
500.00
400.00
300.00
200.00
100.00
0.00
5
10
15
20
25
30
35
40
2theta (°)
100 µm
(b)

Figure 3.

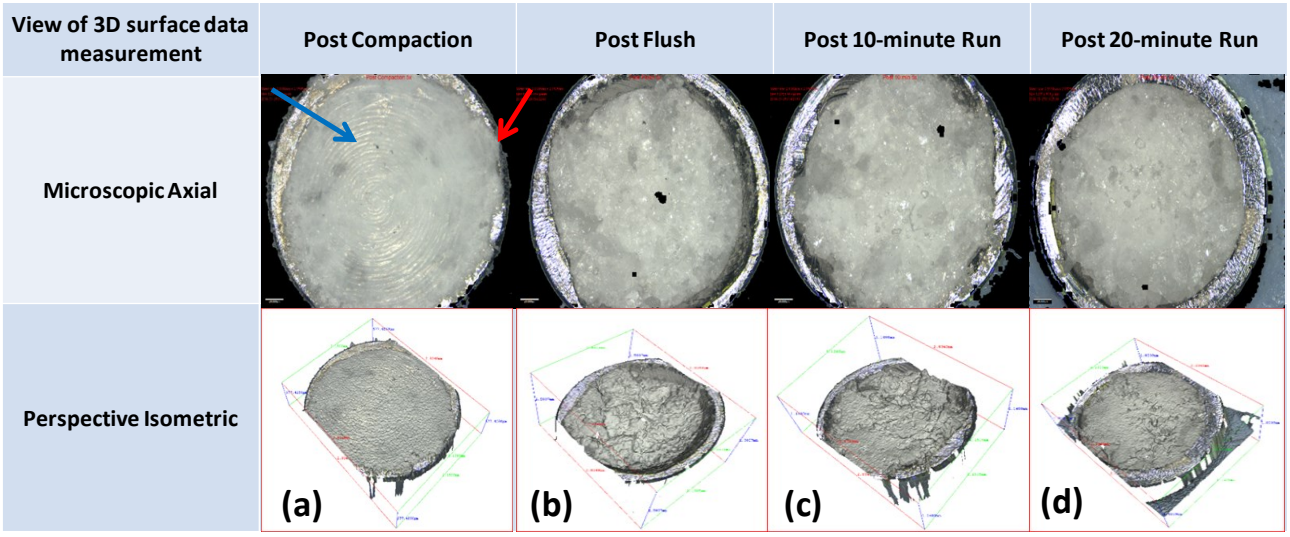
View of 3D surface data measurement
Post Compaction
Post Flush
Post 10-minute Run
Post 20-minute Run
Microscopic Axial
Perspective Isometric
(a)
(b)
(c)
(d)

Figure 4.

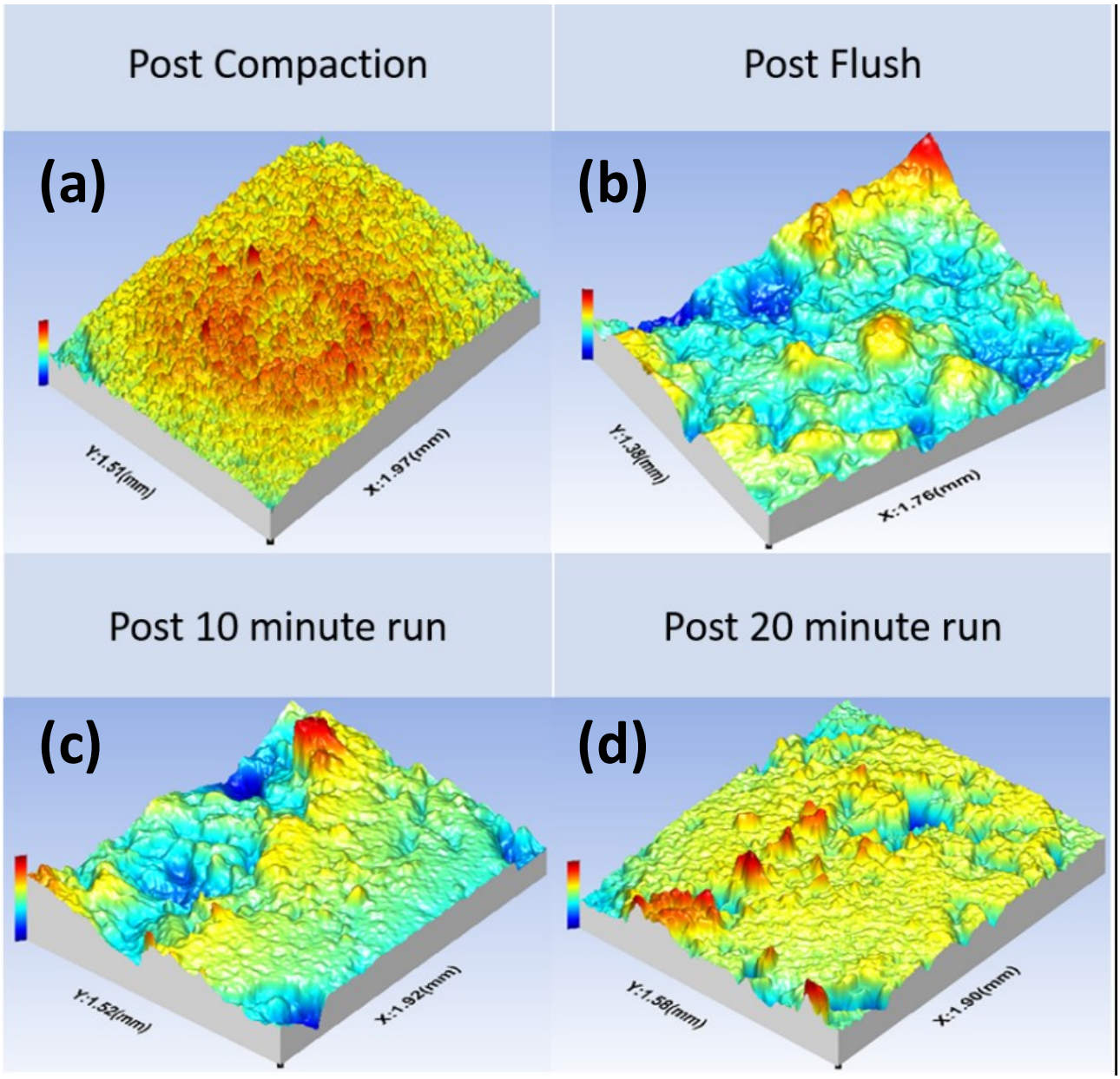
Post Compaction
Post Flush
(a)
(b)
Y:1.51(mm)
X:1.97(mm)
Y:1.38(mm)
X:1.76(mm)
Post 10 minute run
Post 20 minute run
(c)
(d)
Y:1.52(mm)
X:1.92(mm)
Y:1.58(mm)
X:1.90(mm)

Figure 5.